Am J Transl Res 2025;17(6):4689-4700
www.ajtr.org /ISSN:1943-8141/AJTR0164540

Original Article

Undemineralized dentin matrix particles accelerate blood vessel formation in a critical-sized skull defect through activating the TGF-β/PI3K signaling pathway

Wei Zu, Xiangwen Zhou, Qingsong Jiang

Beijing Stomatological Hospital, Capital Medical University, Capital Medical University School of Stomatology, Beijing 100070, China

Received March 14, 2025; Accepted June 1, 2025; Epub June 15, 2025; Published June 30, 2025

Abstract: Objective: To evaluate the effects of undemineralized dentin matrix (UDDM) particles on bone tissue regeneration and vascularization in a critical-sized skull defect (CSD) mouse model, and to elucidate the molecular mechanisms underlying UDDM extract-mediated promotion of endothelial cell proliferation, migration, and tube formation. Methods: UDDM particles and extracts were sourced from human third molars. A CSD mouse model was established, and UDDM particles were implanted into the defect site. Bone regeneration and vascularization (blood vessel volume and area) were assessed using micro-computed tomography (Micro-CT). Human umbilical vein endothelial cells (HUVECs) were treated with UDDM extract and a phosphatidylinositol 3-kinase (PI3K) inhibitor (HY-15244). Cell proliferation, migration, and tube formation were assessed. Reverse transcription quantitative polymerase chain reaction (RT-qPCR) and western blot were used to analyze the expression of transforming growth factor-beta (TGF-β)/PI3K signaling pathway-related genes and proteins. Results: UDDM particles significantly enhanced bone formation and increased vascular volume and area in the CSD model. UDDM extract promoted HUVEC proliferation, migration, and tube formation, which were reversed by HY-15244 treatment. HY-15244 also inhibited the mRNA and protein expression of TGF-β/PI3K pathway components, which were partially rescued by UDDM extract. Conclusion: UDDM particles promote bone tissue regeneration and angiogenesis in a CSD mouse model. UDDM extract facilitates proliferation, migration, and tube formation of HUVECs by activating the TGF-β/PI3K signaling pathway. These findings suggest that UDDM particles and extracts hold promise for therapeutic application in bone defect repair and vascularization.

Keywords: Undemineralized dentin matrix, critical-sized skull defect, HUVEC, blood vessel formation, TGF-β/PI3K signaling pathway

Introduction

Bone tissue repair is a complex and highly regulated process critical for maintaining the structural integrity and physiologic function of the skeletal system [1]. However, critical-sized skull defect (CSD) poses a significant clinical challenge, as these defects exceed the body's intrinsic regenerative capacity and cannot heal spontaneously without medical intervention [2]. Defined as bone loss that fail to undergo complete healing over the organism's lifetime, CSDs commonly result from trauma, degenerative diseases, congenital abnormalities, or surgical resection of tumors [3]. These defects can lead to severe complications, including impaired cranial stability, neurological deficits, and significant aesthetic deformities [4]. The clinical management of CSD is hindered by the limitations of current treatment methods. Traditional approaches, such as autografts and allografts, remain the gold standard; however, they are limited by significant drawbacks, including donor site morbidity, limited tissue availability, potential immune rejection, and suboptimal integration with host tissues [5, 6]. These limitations underscore the urgent need for innovative bone tissue engineering strategies. Recent advancements in synthetic or bio-derived materials, stem cell therapy, and bioactive molecules have shown promise in enhancing bone regeneration [7-9]. Nevertheless, the

https://doi.org/10.62347/OJTK8676

complexity of CSD repair necessitates further exploration into the underlying biological mechanisms and the development of more effective therapeutic strategies.

In recent years, dentin matrix, a bioactive material derived from dental tissues, has gained attention as a promising scaffold for bone tissue regeneration, particularly for treating CSD [10]. Owing to its physicochemical properties and composition, dentin matrix closely resembles bone tissue, containing various growth factors and extracellular matrix proteins such as transforming growth factor-beta (TGF-β), vascular endothelial growth factor (VEGF), and bone morphogenetic proteins (BMPs) [11, 12], which are essential for osteogenesis and bone repair. Dentin matrix can be divided into demineralized dentin matrix (DDM) and undemineralized dentin matrix (UDDM). DDM, characterized by its collagen-rich organic composition and accessible bioactive factors, exhibits superior osteoinductive properties [13]. UDDM, retaining its native mineralized structure, provides enhanced mechanical stability and osteoconductivity [14]. While DDM has been widely studied and is recognized for its dual osteoinductive and osteoconductive properties [13, 15], a key advantage of dentin matrix lies in its low immunogenic and antigenic potential, documented in both autologous and allogeneic transplantation scenarios, thereby ensuring excellent biocompatibility for clinical applications [16]. Studies have shown that DDM outperforms other graft materials in promoting bone tissue repair [17, 18]. However, DDM exhibits inferior mechanical stability compared to UDDM due to the loss of mineral content, leading to premature graft collapse under load-bearing conditions [13]. Furthermore, excessive demineralization accelerates enzymatic collagen degradation, possibly exceeding the rate of new bone formation [13]. These limitations may compromise the overall regenerative outcome, particularly in CSD repair where sustained structural support is essential for successful bone regeneration. Therefore, UDDM, with its enhanced mechanical integrity and osteoconductive properties, may serve as a more suitable graft material for CSD treatment.

Vascularization plays a pivotal role in bone tissue repair and is a key determinant of successful regeneration, particularly in the context of CSD [19]. The establishment of a functional vascular network is essential for delivering oxygen, nutrients, and progenitor cells to the defect site, while facilitating the removal of metabolic waste. In this study, we evaluated the efficacy of human UDDM particles as a bone graft material for CSD repair in a CSD mouse model. Specifically, we investigated the effects and underlying biological mechanisms of UDDM particles in promoting blood vessel formation during the initial phase of bone regeneration. Our study innovatively reveals the dual functionality of UDDM particles in simultaneously enhancing bone formation and early-stage vascularization in CSD, overcoming the single-action limitations of conventional bone graft materials. Moreover, we uncovered a novel molecular mechanism by which UDDM regulates early angiogenic responses, providing mechanistic insight into the pro-vascular properties of dentin-derived biomaterials. Clinically, UDDM represents a safe, cost-effective scaffold for CSD reconstruction, particularly in bone tissue engineering requiring both structural support and enhanced vascularization (e.g., oral-maxillofacial and alveolar ridge regeneration). This study lays the groundwork for the clinical use of UDDM in bone tissue engineering.

Materials and methods

Preparation of human UDDM particles

Dentin samples were sourced from the extracted third molar of patients at the Beijing Stomatological Hospital, Capital Medical University. This study was approved by the Ethics Committee of the Beijing Stomatological Hospital, Capital Medical University, and informed consent was obtained from all participants. Inclusion criteria: patients without periodontal diseases or systemic conditions; exclusion criteria: teeth with caries, periodontitis, visible cracks, or structural anomalies.

Following exaction, the dental follicles, periodontal membrane, enamel, and pulp were thoroughly removed from the exacted teeth through a standardized protocol. After ultrasonic cleaning and sterilization, the remained dentin was crushed using a ball mill (Mixer Mill MM 400, Retsch, Germany) and sieved to obtain powdered UDDM particles. UDDM particles were

stored at -20°C for subsequent experimental use.

Animals

Healthy male C57BL/6 mice (8-10 weeks old) were obtained from the Laboratory Animal Center of Beijing Stomatological Hospital. The animals were housed under standard laboratory environment (23 ± 2°C, 50-55% humidity, and 12-h light-dark cycle) with free access to standard laboratory diet. Mice were randomly assigned to two groups: a control group (CSD mouse model without treatment) and a UDDM group (CSD model treated with sterilized UDDM particles). Animal care was rigorously conducted in accordance with the 3Rs principle (Replacement, Reduction, and Refinement). Animal experimental procedures were approved by the Institutional Animal Care and Use Committee of Beijing Stomatological Hospital, Capital Medical University.

Animal experimental procedures

After a one-week acclimation, the CSD model was established as previously described [10]. Mice were anesthetized by intraperitoneal administration of 100 mg/kg ketamine and 10 mg/kg xylazine. Subsequently, the scalp was shaved and disinfected with povidone-iodine solution. Under aseptic conditions, a 10-15 mm vertical incision was made along the sagittal midline over the parietal bone using sterile instruments. Full-thickness scalp flaps were lifted to expose the calvarium. A 5-mm circular critical-sized defect was created using a trephine bur at slow speed under continuous saline irrigation. The circular bone chip was carefully removed, while preserving the integrity of the underlying dura mater. Following thorough irrigation with sterile normal saline and antibiotic solution, pre-sterilized UDDM particles were implanted into the defect at a density of 1 g/cm^3 in the UDDM group. In the control group, the defects were left untreated. The scalp was closed in layers using 4-0 absorbable silk suture, and the wound was disinfected with povidone-iodine solution. Postoperative care included subcutaneous administration of 0.05 mg/kg buprenorphine for analgesia and 10 mg/kg amoxicillin for infection prophylaxis, administrated once daily for three consecutive days. All animals received standardized postoperative monitoring daily. All mice were euthanized with an intraperitoneal injection of 150 mg/kg pentobarbital sodium at 14 days post-surgery.

Micro-computed tomography (Micro-CT) analysis

At day 14 post-surgery, skull specimens were harvested and fixed in 4% formaldehyde for 48 h. Micro-CT analysis was conducted to assess bone regeneration in the defect region using SkyScan1176 (Bruker, Kontich, Belgium). Scanning parameters were set at 40 kV, 200 μA, 18 μm voxel size, 0.3° rotation step, and 200 ms exposure time. Three-dimensional reconstruction of blood vessels was performed using NRecon and CTvox (Bruker, Kontich, Belgium) software. Quantitative analysis of vascular volume and area was conducted using CTanalyzer. Bone regeneration was evaluated by calculating bone volume fraction (bone volume/tissue volume, BV/TV), bone surface/total volume (BS/TV), bone surface/bone volume (BS/BV), and trabecular thickness (Tb.Th).

Evaluation of blood vessel formation

At 14 days post-surgery, vascular perfusion was performed using Microfil (MV-122; Flow Tech, Carver, MA, USA) and blood vessel formation was subsequently assessed via Micro-CT according to established protocols [20]. In brief, mice were deeply anesthetized by intraperitoneal administration of 150 mg/kg pentobarbital sodium, and a midline incision was made from the xiphoid process to the lower abdomen to expose the heart. Heparin (5.000 U/mL, 300 μL) was injected directly into the left ventricle. After 10 min, the left ventricle was catheterized, and the right atrium was incised for blood drainage. Subsequently, the vasculature was perfused with 20 mL of heparinized saline (100 U/mL) at a rate of 2 mL/min. Then, 3 mL of the Microfil solution was prepared and perfused at 2 mL/min via the intracardiac canula. After perfusion, the aorta and inferior vena cava were immediately ligated, and the mice were stored at 4°C overnight. Finally, the entire skull was carefully dissected and fixed in 4% paraformaldehyde for 24 h. The skull samples were decalcified in 10% Ethylene diamine tetra acetic acid (EDTA) solution for 4 weeks prior to Micro-CT analysis. Micro-CT analysis was conducted to assess blood vessel formation using SkyScan1176 (Bruker, Kontich, Belgium) based

on the methods mentioned above. The blood vessel volume and area were quantified.

Preparation of UDDM extract

To prepare UDDM extracts at two distinct concentrations, UDDM particles were immersed in PBS at ratios of 10 g per 30 mL and incubated at 37°C for 24 h with constant shaking. Afterwards, the resulting suspension was centrifuged at 10,000 rpm for 10 min at 4°C to remove insoluble particles. The supernatant was aseptically filtered through a 0.2 μm syringe filter to obtain the UDDM extract, which was stored at 4°C until further use.

Enzyme-linked immunosorbent assay (ELISA)

The concentration of TGF-β in the UDDM extract was quantified using TGF-β ELISA kit (Elabscience Wuhan, China) following the manufacturer's instructions.

Cell culture and treatment

Human umbilical vein endothelial cells (HUVECs) were sourced from American Type Culture Collection (ATCC, Manassas, VA, USA) and cultured in Dulbecco's modified Eagle medium (DMEM) supplemented with 10% fetal bovine serum and antibiotics at 37°C in 5% CO_2. The prepared UDDM extract was diluted with complete DMEM at a ratio of 1:5 for cell culture. When HUVECs reached 70% confluence, they were randomly divided into three groups: control group (cultured in complete DMEM), UDDM group (cultured in diluted UDDM extract), and UDDM+HY-15244 group (cultured in diluted UDDM extract with addition of the PI3K inhibitor HY-15244). The culture medium was replaced every 24 hours.

Cell Counting Kit-8 (CCK-8) assay

HUVEC suspensions were seeded in 96-well plates at 5×10^3 cells/well and maintained under standard culture conditions. Following incubation periods of 0, 24, 48, and 72 hours, 10 μL of CCK-8 reagent (Beyotime, Shanghai, China) was added to each well and incubated for 2 h. Afterwards, the absorbance at 450 nm was examined using a microplate reader (Bio-Rad, USA) to evaluate cell proliferation.

Wound healing migration assay

For wound healing assay, 6-well culture plates were pre-marked with reference lines perpendicular to the base. HUVECs from each experimental group were seeded and grown to ~70% confluence. A uniform scratch was created across each well using a sterile 100 μL pipette tips, ensuring orientation perpendicular to the reference markers. After removing cellular debris through three PBS washes, serum-free medium was added to each well, and the plates were maintained in culture conditions for 12 hours. Wound closure was documented at predetermined intervals using microscopy, and quantitative analysis was performed using ImageJ analysis software to assess cell migration.

Tube formation assay

Angiogenic potential was assessed using a tube formation assay. Specifically, 1×10^4 HUVECs were plated into 96-well plates that pre-coated with 50 μL of Matrigel and incubated at 37°C in 5% CO_2 overnight. The cell medium was then replaced with conditioned medium collected from HUVECs in each experimental group. Tube formation was observed under a microscope and analyzed using ImageJ software.

Reverse transcription quantitative polymerase chain reaction (RT-qPCR)

HUVECs were lysed using TRIzol reagent and total RNA was extracted. The cDNA was synthesized from the extracted RNA using PrimeScript RT reagent (Takara, Dalian, China). RT-qPCR was performed in a 20 μL reaction volume using SYBR Green kit (TaKaRa, Dalian, China) on an ABI 7500 system (Thermo Fisher, USA). The mRNA expression was normalized to GAPDH and quantified using the $2^{-\Delta\Delta CT}$ method. The primer sequences are listed in **Table 1**.

Western blot analysis

Intracellular proteins were extracted from HUVECs using RIPA buffer. Proteins were separated by 10% sodium dodecyl sulfate - polyacrylamide gel electrophoresis (SDS-PAGE) and transferred onto polyvinylidene fluoride (PVDF) membranes (Millipore, USA). The membranes were blocked with 5% non-fat milk and incubat-

Table 1. The primer sequences in reverse transcription quantitative polymerase chain reaction (RT-qPCR) assay

Gene	Primer sequences	
p100α	forward	5'-CCACGACCATCATCAGGTGAA-3'
	reverse	5'-CCTCACGGAGGCATTCTAAAGT-3'
p100β	forward	5'-AGAGCACTTGGTAATCGGAGG-3'
	reverse	5'-CTTCCCCGGCAGTATGCTTC-3'
p100δ	forward	5'-TCAACTCACAGATCAGCCTCC-3'
	reverse	5'-CGCGAAAGTCGTTCACTTCT-3'
phosphatidylinositol (3,4,5)-trisphosphate (PIP3)	forward	5'-AACACCGACCTCACAGTTTTT-3'
	reverse	5'-CTCAAGCCACACATTCCACAG-3'
Protein kinase B (AKT)	forward	5'-AGCGACGTGGCTATTGTGAAG-3'
	reverse	3'-GCCATCATTCTTGAGGAGGAAGT-5'
Glyceraldehyde-3-phosphate dehydrogenase (GAPDH)	forward	5'-ACGGATTTGGTCGTATTGGG-3'
	reverse	5'-GGGATCTCGCTCCTGGAAG-3'

ed overnight at 4°C with specific primary antibodies (1:1000 dilution), followed by incubation with HRP-conjugated secondary antibody for 2 h. The protein bands were visualized using enhanced chemiluminescence (ECL) substrate (Pierce, IL, USA) and quantified with ImageJ analysis software. The primary antibodies used included p100α (ab127617, Abcam), p100β (ab151549, Abcam), p100δ (ab109006, Abcam), phosphatidylinositol-4,5-bisphosphate 3-kinase catalytic subunit gamma (PIK3CG) (ab302958, Abcam), protein kinase B (AKT) (#4691, Cell Signaling Technology), and glyceraldehyde-3-phosphate dehydrogenase (GAPDH) (ab181602, Abcam).

Statistical analysis

Data derived from three distinct experimental trials were expressed as mean ± standard deviation (SD). Statistical analyses were performed using SPSS 22.0. Intergroup comparisons between two groups were conducted using Student's t-test, while comparisons among multiple groups were performed using one-way ANOVA followed by Tukey-Kramer correction. Statistical significance was determined at $P<0.05$.

Results

UDDM particles promoted bone tissue repair and blood vessel formation in the skull of CSD mouse model

To assess the effects of UDDM particles on vascularization during bone regeneration, a CSD mouse model was established and UDDM particles were implanted into the defects. At 14 days post-operation, no signs of abnormal healing were observed in either group, suggesting good biocompatibility of the UDDM particles (**Figure 1A**). Micro-CT analysis revealed significantly increased values of BV/TV (**Figure 1B**), BS/TV (**Figure 1C**), and Tb.Th (**Figure 1D**), alongside a reduction in BS/BV (**Figure 1E**), indicating enhanced bone formation and improved bone tissue repair. Additionally, Micro-CT imaging showed a higher density of newly formed blood vessels in the UDDM group than the control group (**Figure 1F**). Both blood vessel volume (**Figure 1G**) and area (**Figure 1H**) significantly increased following UDDM treatment. Our results revealed that UDDM particles promoted both bone repair and neovascularization in the CSD model.

UDDM extract facilitated HUVEC proliferation

To elucidate the molecular mechanisms of UDDM particles in blood vessel formation, UDDM extract was prepared and used to treat HUVECs *in vitro*. ELISA revealed that TGF-β was the only detectable growth factor in the extract, with a concentration of 49.6 pg/mL in the 1:5 diluted solution. Given the established role of the TGF-β/phosphatidylinositol 3-kinase (PI3K) signaling pathway in wound healing processes [21], we hypothesized that this pathway mediates the effects of UDDM extract.

To verify this, we then investigated the molecular mechanisms of UDDM extract in bone defect repair using a PIK3 inhibitor HY-15244. CCK-8

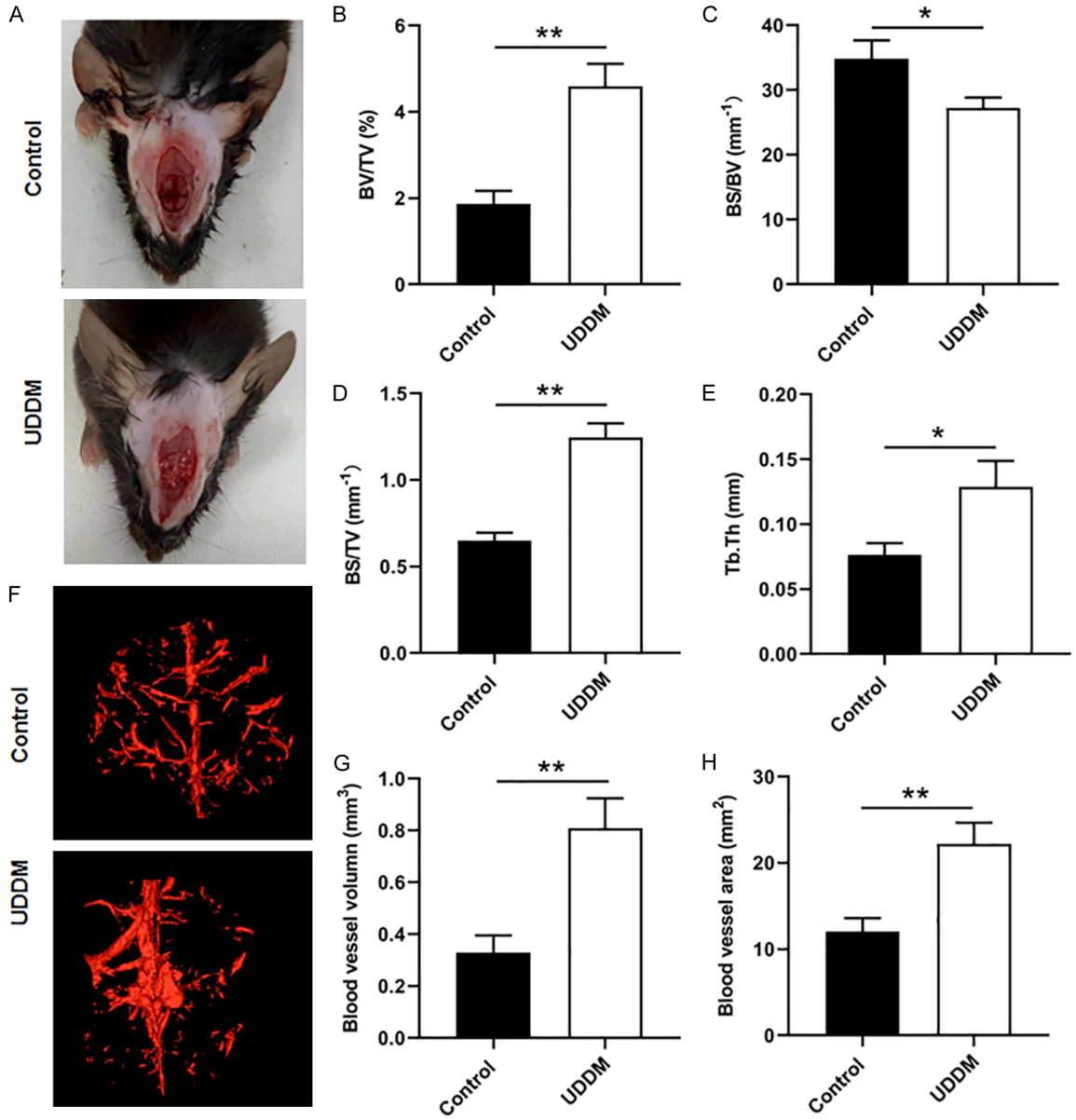

Figure 1. Undemineralized dentin matrix (UDDM) particles promoted bone tissue repair and blood vessel formation in the skull of critical-sized skull defect (CSD) mouse model. A CSD mouse model was established and UDDM particles were implanted into the defect. (A) The photograph of the surgical area in two groups at 7 days post-operation. (B) Bone volume/tissue volume (BV/TV) (%), (C) bone surface/total volume (BS/TV), (D) trabecular thickness (Tb.Th), and (E) bone surface/bone volume (BS/BV) were quantified by using the Micro-computed tomography (Micro-CT) analysis. (F) The blood vessel formation in two groups were assessed using Micro-CT analysis. (G) The quantification of blood vessel volume and (H) blood vessel area. Data were presented as mean ± standard deviation (SD). *P<0.05, **P<0.01.

assay results illustrated that UDDM extract significantly enhanced HUVEC proliferation, whereas co-treatment with HY-15244 abolished this effect (**Figure 2**). These findings suggest that UDDM extract promotes cell proliferation through activation of the TGF-β/PI3K signaling pathway.

UDDM extract facilitated HUVEC migration

To evaluate the effect of UDDM extract on endothelial cell migration, HUVECs were subjected to wound healing assays following treatment with UDDM extract or HY-15244. At 24 hours post-scratch, enhanced wound healing

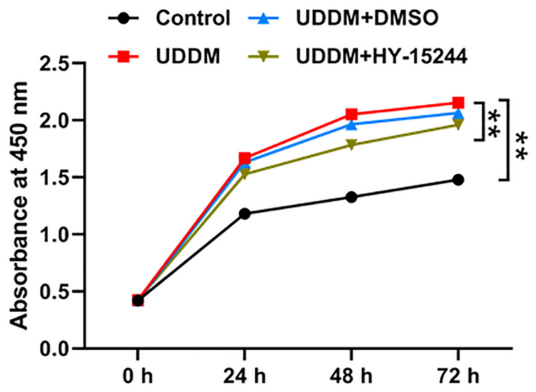

Figure 2. UDDM extract facilitated cell proliferation in human umbilical vein endothelial cells (HUVECs). Data were presented as mean ± SD. $^{**}P<0.01$.

was observed in the UDDM group compared with the control group (**Figure 3A**, **3B**). However, HY-15244 treatment prominently eliminated the stimulatory effect of UDDM extract on HUVEC migration. Our results indicate that UDDM extract facilitates HUVEC migration by activating the TGF-β/PI3K signaling pathway.

UDDM extract facilitated blood vessel formation in HUVECs

The angiogenic potential of UDDM extract was further evaluated *in vitro* using the tube formation assay. Representative images of the vascular networks following 4, 8, and 12 hours of incubation are shown in **Figure 4A**. At the 8-hour time point, HUVECs in the UDDM group exhibited mature and well-organized tubular structures, whereas cells in the control group formed incomplete and irregular networks, with partial cell aggregation into sheet-like structures. Quantitative analysis revealed that UDDM extract markedly increased tube length and branch number compared with the control group at all time points (4, 8, and 12 h) (**Figure 4B**, **4C**). However, HY-15244 treatment abrogated these effects. Collectively, UDDM extract promotes in vitro angiogenesis in HUVECs by activating the TGF-β/PI3K signaling pathway.

UDDM extract activated of the TGF-β/PI3K signaling pathway in HUVECs

To confirm the involvement of the TGF-β/PI3K signaling pathway, we analyzed the expression of key pathway components at both the mRNA and protein levels. RT-qPCR results demonstrated that HY-15244 treatment significantly downregulated the mRNA expression of TGF-β/PI3K signaling pathway-related genes, including PI3K p100α, PI3K p100β, PI3K p100δ, phosphatidylinositol (3,4,5)-trisphosphate (PIP3) and AKT, while co-treatment with UDDM extract (1:5) abrogated these effects (**Figure 5A-E**). Similarly, HY-15244 treatment reduced the protein expressions of p100α, p100β, p100δ, PIK3CG, and AKT, which were then reversed by UDDM extract treatment (**Figure 5F-K**). Together, these results demonstrate that UDDM extract activates the TGF-β/PI3K signaling pathway in HUVECs, thereby promoting wound healing and blood vessel formation.

Discussion

In critical-sized bone defects, impaired vascularization severely disrupts the natural healing process, leading to incomplete or failed regeneration and posing a substantial challenge in clinical treatment. This highlights the need for therapeutic strategies that effectively promote vascularization to support bone repair in CSD management. Our findings provide compelling evidence for the dual pro-angiogenic and osteogenic potential of UDDM in CSD repair. The experimental results demonstrated that UDDM particles significantly enhanced bone formation and promoted neovascularization in a CSD mouse model, a critical step for successful bone regeneration. These effects were further supported by in vitro experiments where UDDM extract significantly enhanced the proliferation, migration, and blood vessel formation in HUVECs, suggesting its potential to stimulate multiple phases of blood vessel formation. These findings are consistent with previous studies highlighting the pivotal role of vascularization in bone tissue engineering, particularly for critical-sized defects where the intrinsic vascular supply is severely damaged [22, 23]. UDDM exhibits dual pro-angiogenic and osteogenic effects in CSD, addressing the critical challenge of vascular insufficiency in CSD repair that hinders natural healing.

The differential regenerative properties of DDM and UDDM on bone regeneration have been well documented. DDM exhibits superior osteoinductive capacity through the exposure of bioactive factors such as BMPs and TGF-β following demineralization, with demonstrated regenerative osteogenic potential in a CSD model

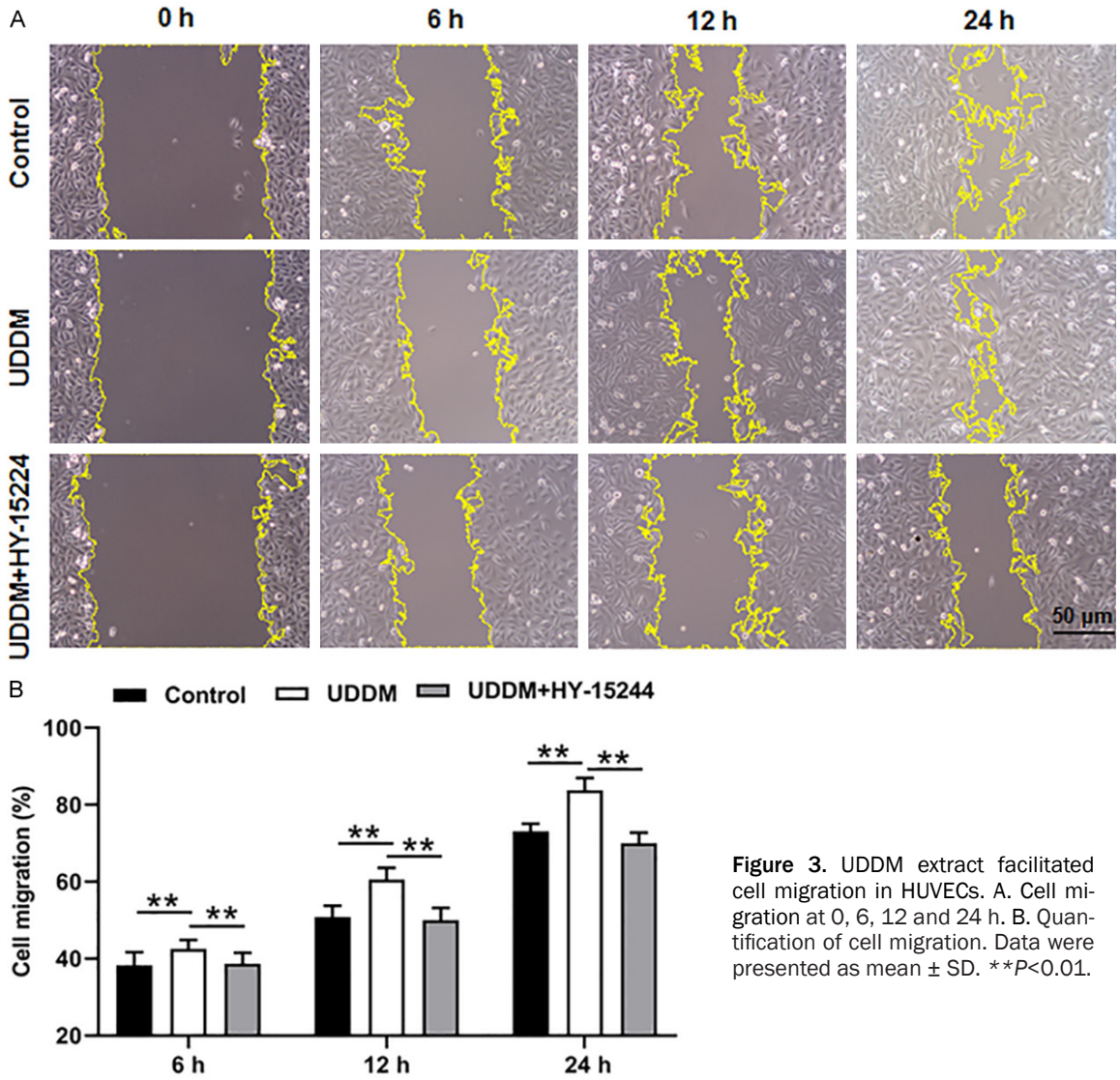

Figure 3. UDDM extract facilitated cell migration in HUVECs. A. Cell migration at 0, 6, 12 and 24 h. B. Quantification of cell migration. Data were presented as mean ± SD. $^{**}P<0.01$.

[24, 25]. However, excessive demineralization may compromise the structural integrity of DDM, leading to accelerated resorption and potential graft failure, particularly in load-bearing applications [13]. In comparison, UDDM maintains its native mineralized structure, providing enhanced mechanical stability and a controlled release of growth factors, making it more suitable for defects requiring structural integrity. This may explain its sustained pro-angiogenic effects observed in our study. Notably, the partially demineralized dentin matrix (PDDM) has been identified as a promising intermediate, combining the advantages of both DDM and UDDM. Studies have shown that PDDM maintains sufficient mechanical strength while partially exposing bioactive factors, resulting in a balanced osteoinductive-osteoconductive profile [26]. Our findings highlight that UDDM balances structural integrity and sustained growth factor release, making it an optimal graft material in bone tissue engineering for critical-size defects.

The therapeutic effects of UDDM are primarily mediated by the gradual release of growth factors from its mineralized matrix throughout the remodeling process, thereby supporting sustained angiogenesis and osteogenesis. Our findings demonstrated that UDDM extract activates the TGF-β/PI3K signaling pathway in HUVECs, offering mechanistic insights into its pro-angiogenic effects. Notably, TGF-β serves as a key regulator of both angiogenesis and

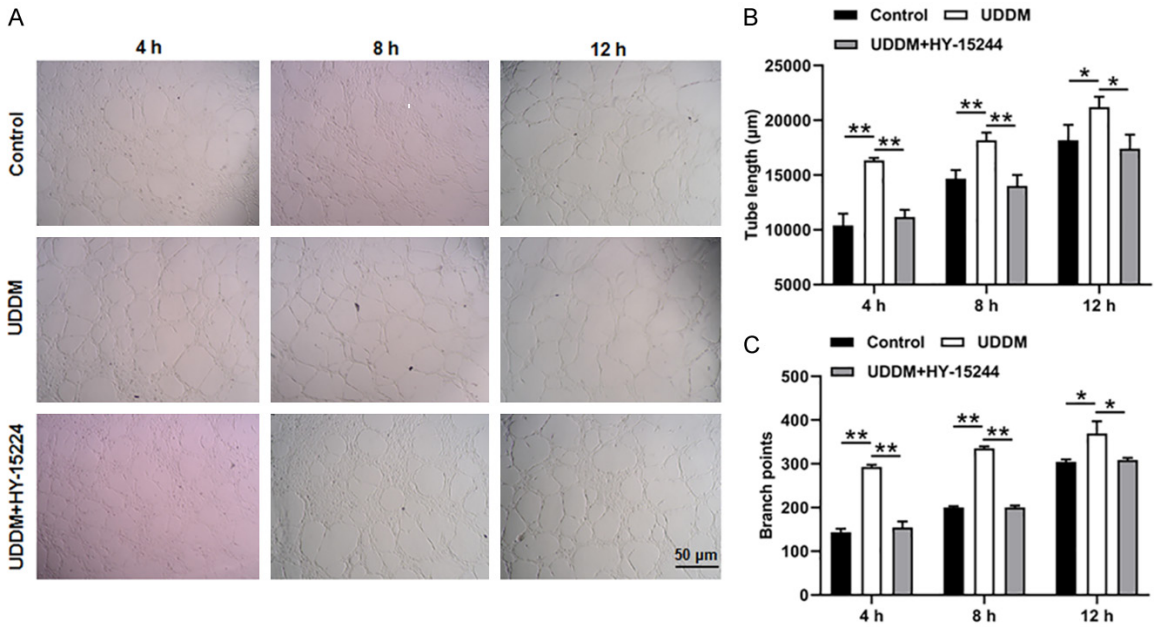

Figure 4. UDDM extract facilitated blood vessel formation in HUVECs. (A) Representative images of the vascular networks following 4, 8, and 12 hours of incubation. (B) The tube length and (C) branch number were quantified for each group. Data were presented as mean ± SD. *P<0.05, **P<0.01.

osteogenesis [27]. UDDM-induced activation of the TGF-β/PI3K pathway aligns with previous studies demonstrating that TGF-β signaling enhances endothelial cell proliferation, migration, and tube formation, all of which are essential for vascular network formation during bone repair [28]. The observed activation of the TGF-β/PI3K pathway by UDDM suggests this axis contributes significantly to its angiogenic function. Moreover, this pathway is known to interact with other osteogenesis-related pathways, including BMP and MAPK signaling [29, 30], suggesting crosstalk that may create a synergistic microenvironment conducive to both vascularization and bone regeneration. Although the osteoinductive properties of UDDM have been well-documented, its angiogenic potential remains relatively unexplored. Notably, our results reveal that the pro-angiogenic mechanism of UDDM involves TGF-β/PI3K pathway activation, linking vascularization to osteogenesis through synergistic signaling crosstalk. We highlight a distinct advantage of UDDM in promoting early-stage vascularization, a critical determinant for successful bone regeneration, particularly in critical-sized defects.

This study had several limitations. First, the mouse CSD model may not fully recapitulate the complexity of human bone repair processes, necessitating validation in larger preclinical models. Second, the study focused on short-term outcomes (14 days post-implantation), leaving the long-term fate of UDDM grafts and vascular network maturation unexplored. Third, other possible molecule mechanisms by which UDDM regulates vascularization were not thoroughly investigated. Future investigations should evaluate the remodeling kinetics and biomechanical performance of UDDM over extended periods. Comparative analyses between UDDM and PDDM may help determine the optimal demineralization degree for balancing mechanical stability and bioactivity. Finally, clinical trials are essential to confirm the efficacy of UDDM in human bone defect repair and to establish standardized clinical protocols.

In summary, our results demonstrate that UDDM particles enhance bone formation and promote blood vessel formation in a CSD mouse model by activating the TGF-β/PI3K signaling pathway. These results suggest that UDDM could serve as a promising biomaterial for bone tissue engineering, particularly in applications requiring both structural integrity and vascular support. The dual role of UDDM in promoting angiogenesis while maintaining mechanical stability makes it particularly suit-

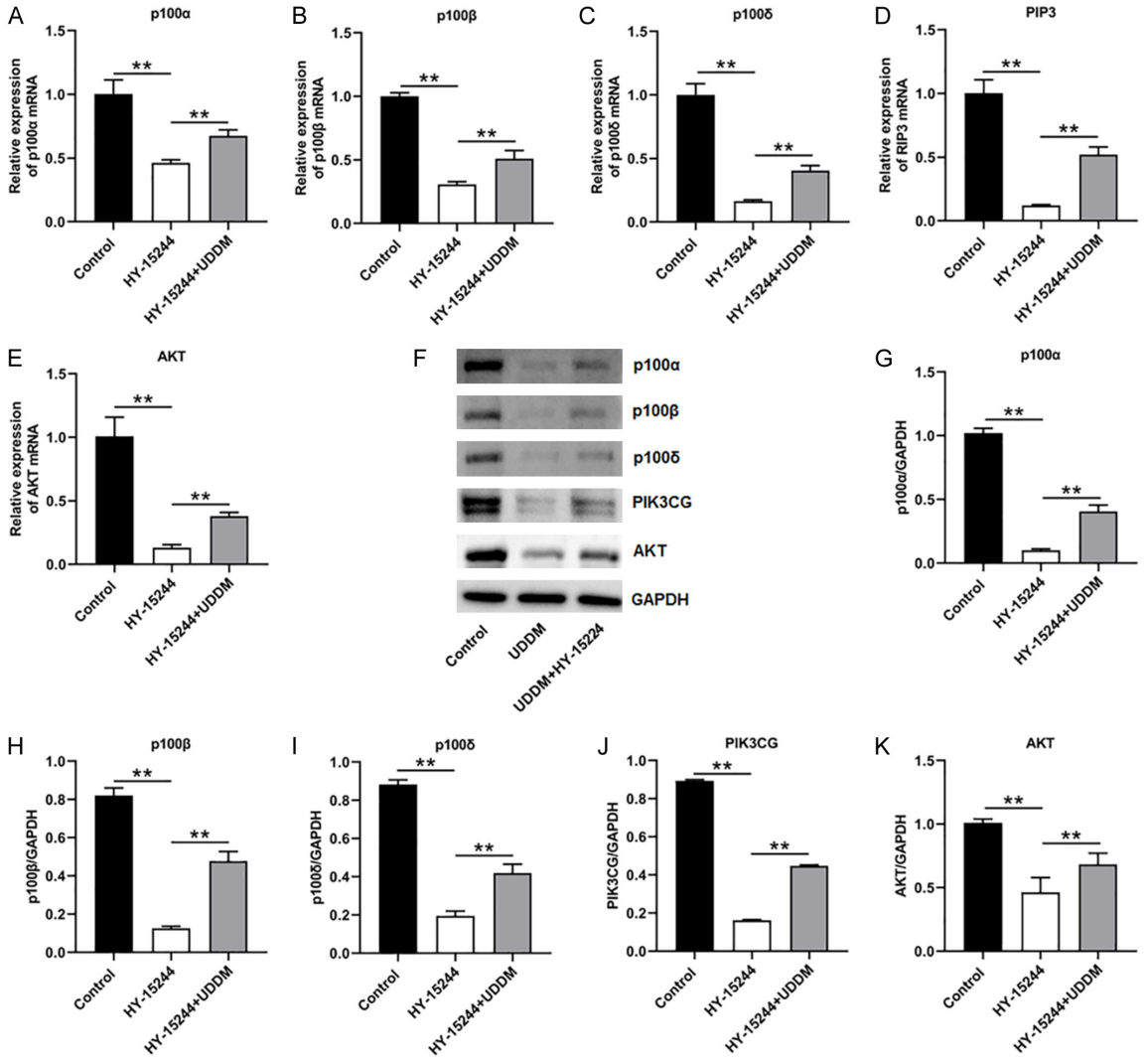

Figure 5. UDDM extract promoted the activation of the TGF-β/phosphatidylinositol 3-kinase (PI3K) signaling pathway in HUVECs. A-E. The mRNA expression of PI3K p100α, PI3K p100β, PI3K p100δ, phosphatidylinositol (3,4,5)-trisphosphate (PIP3), and protein kinase B (AKT) was examined using RT-qPCR. F-K. The protein expression of PI3K p100α, PI3K p100β, PI3K p100δ, phosphatidylinositol-4,5-bisphosphate 3-kinase catalytic subunit gamma (PIK3CG), and protein kinase B (AKT) was assessed using western blot analysis. Data were presented as mean ± SD. $^{**}P<0.01$.

able for treating CSD. Our findings lay a foundation for the clinical translation of UDDM as a safe, effective, and cost-efficient biomaterial in bone tissue engineering.

Disclosure of conflict of interest

None.

Abbreviations

UDDM, Undemineralized dentin matrix; DDM, demineralized dentin matrix; CSD, critical-sized skull defect; HUVECs, Human umbilical vein endothelial cells.

Address correspondence to: Qingsong Jiang, Beijing Stomatological Hospital, Capital Medical University, Capital Medical University School of Stomatology, No. 9 Fanjiacun Road, Fengtai District, Beijing 100070, China. E-mail: qsjiang@ccum.edu.cn

References

[1] Salhotra A, Shah HN, Levi B and Longaker MT. Mechanisms of bone development and repair. Nat Rev Mol Cell Biol 2020; 21: 696-711.

[2] Huang EE, Zhang N, Shen H, Li X, Maruyama M, Utsunomiya T, Gao Q, Guzman RA and Goodman SB. Novel techniques and future perspective for investigating critical-size

bone defects. Bioengineering (Basel) 2022; 9: 171.
[3] Nauth A, Schemitsch E, Norris B, Nollin Z and Watson JT. Critical-size bone defects: is there a consensus for diagnosis and treatment? J Orthop Trauma 2018; 32 Suppl 1: S7-S11.
[4] Johnson ZM, Yuan Y, Li X, Jashashvili T, Jamieson M, Urata M, Chen Y and Chai Y. Mesenchymal stem cells and three-dimensional-osteoconductive scaffold regenerate calvarial bone in critical size defects in swine. Stem Cells Transl Med 2021; 10: 1170-1183.
[5] Baldwin P, Li DJ, Auston DA, Mir HS, Yoon RS and Koval KJ. Autograft, allograft, and bone graft substitutes: clinical evidence and indications for use in the setting of orthopaedic trauma surgery. J Orthop Trauma 2019; 33: 203-213.
[6] Migliorini F, Maffulli N, Baroncini A, Eschweiler J, Knobe M, Tingart M and Schenker H. Allograft versus autograft osteochondral transplant for chondral defects of the talus: systematic review and meta-analysis. Am J Sports Med 2022; 50: 3447-3455.
[7] Dec P, Modrzejewski A and Pawlik A. Existing and novel biomaterials for bone tissue engineering. Int J Mol Sci 2022; 24: 529.
[8] Wang J, Liu M, Yang C, Pan Y, Ji S, Han N and Sun G. Biomaterials for bone defect repair: types, mechanisms and effects. Int J Artif Organs 2024; 47: 75-84.
[9] Tam WL, Freitas Mendes L, Chen X, Lesage R, Van Hoven I, Leysen E, Kerckhofs G, Bosmans K, Chai YC, Yamashita A, Tsumaki N, Geris L, Roberts SJ and Luyten FP. Human pluripotent stem cell-derived cartilaginous organoids promote scaffold-free healing of critical size long bone defects. Stem Cell Res Ther 2021; 12: 513.
[10] Li YF, Luo QP, Yang YX, Li AQ and Zhang XC. A novel bi-layered asymmetric membrane incorporating demineralized dentin matrix accelerates tissue healing and bone regeneration in a rat skull defect model. Biomater Sci 2024; 12: 4226-4241.
[11] Anumula L, Ramesh S and Kolaparthi VSK. Matrix metalloproteinases in dentin: assessing their presence, activity, and inhibitors - a review of current trends. Dent Mater 2024; 40: 2051-2073.
[12] Chen J, Liao L, Lan T, Zhang Z, Gai K, Huang Y, Chen J, Tian W and Guo W. Treated dentin matrix-based scaffolds carrying TGF-β1/BMP4 for functional bio-root regeneration. Applied Materials Today 2020; 20: 100742.
[13] Grawish ME, Grawish LM, Grawish HM, Grawish MM, Holiel AA, Sultan N and El-Negoly SA. Demineralized dentin matrix for dental and alveolar bone tissues regeneration: an innovative scope review. Tissue Eng Regen Med 2022; 19: 687-701.
[14] Lee B, Choi H and Sohn DS. Optimizing bone regeneration with demineralized dentin-derived graft material: impact of demineralization duration in a rabbit calvaria model. J Funct Biomater 2024; 15: 331.
[15] Khurshid Z, Adanir N, Ratnayake J, Dias G and Cooper PR. Demineralized dentin matrix for bone regeneration in dentistry: a critical update. Saudi Dent J 2024; 36: 443-450.
[16] Um IW, Lee JK, Kim JY, Kim YM, Bakhshalian N, Jeong YK and Ku JK. Allogeneic dentin graft: a review on its osteoinductivity and antigenicity. Materials (Basel) 2021; 14: 1713.
[17] Ouyang L, Li J, Dong Y, Li J, Jin F, Luo Y, Wang R and Wang S. Comparison of clinical efficacy between autologous partially demineralized dentin matrix and deproteinized bovine bone mineral for bone augmentation in orthodontic patients with alveolar bone deficiency: a randomized controlled clinical trial. BMC Oral Health 2024; 24: 984.
[18] Sohn DS and Moon YS. Histomorphometric study of rabbit's maxillary sinus augmentation with various graft materials. Anat Cell Biol 2018; 51 Suppl 1: S1-S12.
[19] Ren Y, Chu X, Senarathna J, Bhargava A, Grayson WL and Pathak AP. Multimodality imaging reveals angiogenic evolution in vivo during calvarial bone defect healing. Angiogenesis 2024; 27: 105-119.
[20] Caliaperoumal G, Souyet M, Bensidhoum M, Petite H and Anagnostou F. Type 2 diabetes impairs angiogenesis and osteogenesis in calvarial defects: MicroCT study in ZDF rats. Bone 2018; 112: 161-172.
[21] Zhang Z, Zhang X, Zhao D, Liu B, Wang B, Yu W, Li J, Yu X, Cao F, Zheng G, Zhang Y and Liu Y. TGF-β1 promotes the osteoinduction of human osteoblasts via the PI3K/AKT/mTOR/S6K1 signalling pathway. Mol Med Rep 2019; 19: 3505-3518.
[22] Han Y, Wu Y, Wang F, Li G, Wang J, Wu X, Deng A, Ren X, Wang X, Gao J, Shi Z, Bai L and Su J. Heterogeneous DNA hydrogel loaded with Apt02 modified tetrahedral framework nucleic acid accelerated critical-size bone defect repair. Bioact Mater 2024; 35: 1-16.
[23] Yang Z, Yang Z, Ding L, Zhang P, Liu C, Chen D, Zhao F, Wang G and Chen X. Self-adhesive hydrogel biomimetic periosteum to promote critical-size bone defect repair via synergistic osteogenesis and angiogenesis. ACS Appl Mater Interfaces 2022; 14: 36395-36410.
[24] Sultan N and Jayash SN. In vivo evaluation of regenerative osteogenic potential using a human demineralized dentin matrix for dental application. Dent J (Basel) 2024; 12: 76.

[25] Kim BJ, Kim SK and Lee JH. Bone regeneration of demineralized dentin matrix with platelet-rich fibrin and recombinant human bone morphogenetic protein-2 on the bone defects in rabbit calvaria. Maxillofac Plast Reconstr Surg 2021; 43: 34.

[26] Koga T, Minamizato T, Kawai Y, Miura K, I T, Nakatani Y, Sumita Y and Asahina I. Bone regeneration using dentin matrix depends on the degree of demineralization and particle size. PLoS One 2016; 11: e0147235.

[27] Bonnici L, Suleiman S, Schembri-Wismayer P and Cassar A. Targeting signalling pathways in chronic wound healing. Int J Mol Sci 2023; 25: 50.

[28] Liu H, Sun M, Wu N, Liu B, Liu Q and Fan X. TGF-β/Smads signaling pathway, Hippo-YAP/TAZ signaling pathway, and VEGF: their mechanisms and roles in vascular remodeling related diseases. Immun Inflamm Dis 2023; 11: e1060.

[29] Hiepen C, Mendez PL and Knaus P. It takes two to tango: endothelial TGFβ/BMP signaling crosstalk with mechanobiology. Cells 2020; 9: 1965.

[30] Vlashi R, Zhang X, Wu M and Chen G. Wnt signaling: essential roles in osteoblast differentiation, bone metabolism and therapeutic implications for bone and skeletal disorders. Genes Dis 2022; 10: 1291-1317.